

# Tensor Decomposition for Spatiotemporal Mobility Pattern Learning with Mobile Phone Data

 Transportation Research Record  
 1–14

© The Author(s) 2024

Article reuse guidelines:

sagepub.com/journals-permissions

DOI: 10.1177/03611981241270166

journals.sagepub.com/home/trr


 Suxia Gong<sup>1</sup> , Ismaïl Saadi<sup>2</sup> , Jacques Teller<sup>1</sup>, and Mario Cools<sup>1,3,4</sup>

## Abstract

Detecting urban mobility patterns is crucial for policymakers in urban and transport planning. Mobile phone data have been increasingly deployed to measure the spatiotemporal variations in human mobility. This work applied non-negative Tucker decomposition (NTD) to mobile phone-based origin–destination (O-D) matrices to explore mobility patterns' latent spatial and temporal relationships in the province of Liège, Belgium. Four  $310 \times 310 \times 24$  traffic tensors have been built for one regular weekday, one regular weekend day, one holiday weekday, and one holiday weekend day, respectively. The proposed method inferred spatial clusters and temporal patterns while interpreting the correlation between spatial clusters and temporal patterns through geographical visualization. As a result, we found the similarity of O-D and destination–origin (D-O) patterns and the symmetry for the trips of the temporal patterns with evening peak and morning peaks on the weekday. Moreover, we investigated the attraction of different spatial clusters with two temporal patterns on a regular weekday and validated the reconstructed demand using population counts and commuting matrices. Finally, the differences in spatial and temporal interactions have been addressed in detail.

## Keywords

Mobile phone data, OD matrices, Mobility patterns, Non-negative Tucker decomposition

Mobile phone data have been increasingly applied to measure the spatiotemporal changes in population because of its cost effectiveness and high penetration rate compared with conventional survey methods (1–3). Even though the data have shortcomings, such as positioning uncertainty and the lack of sociodemographic information on mobile phone users, they represent a reasonable proxy for individual mobility and show enormous potential as an alternative in urban transport modeling (4). Mobile phone-based origin–destination (O-D) matrices are often generated from the cell phone source data for further strategic planning. Based on O-D matrices, it is possible to draw up a “mobility map” showing the number of people moving between different locations of a designed network over a given temporal period. Additionally, we can find the underlying influence of land use on human mobility by combining traffic flow with land use conditions (5). The discovery can explain the urban spatiotemporal structure and support policymakers in making decisions during emergencies related

to human mobility. Studies such as Gibbs et al. (6), Fan et al. (7), and Awad-Núñez et al. (8) show that epidemics or catastrophic emergencies can lead to a fluctuation in human mobility patterns. Thus, modeling and understanding human mobility before, during, or after a disaster is crucial. One of the challenges of learning human mobility patterns lies in the simultaneous interpretation of spatial and temporal interactions, especially for dynamic and large-scale traffic networks. Many efforts have been made with different kinds of data to model

<sup>1</sup>LEMA Research Group, Department of Urban & Environmental Engineering, University of Liège, Liège, Belgium

<sup>2</sup>MRC Epidemiology Unit, School of Clinical Medicine, University of Cambridge, Cambridge, UK

<sup>3</sup>Faculty of Business Economics, Hasselt University, Diepenbeek, Belgium

<sup>4</sup>Department of Mathematics, Education, Econometrics and Statistics (MEES), KULeuven Campus Brussels, Belgium

## Corresponding Author:

 Suxia Gong, [suxia.gong@uliege.be](mailto:suxia.gong@uliege.be)

urban spatiotemporal structures, such as the spatiotemporal distribution of activity intensity (9) or the evolution of link-based traffic flow (10, 11). In addition, Furtlehner et al. (12) applied synthetic floating car data to cluster an urban road network with congestion problems, aiming at extracting large-scale spatial and temporal features of road traffic. Sun et al. (13) used smart card data to extract passengers' spatiotemporal density based on a regression model. Jiang et al. (14) employed travel surveys to mine the spatiotemporal activity patterns by combining the clusters of individuals with the spatial dimension. These studies have expanded the traditional understanding of urban structure from the spatial dimension based on static density to the dynamic spatiotemporal dimension. However, despite the multidimensional data sets, their methods mostly deal with two-dimensional data (15) and cannot efficiently interpret spatiotemporal dependencies.

Multidimensional tensors have recently found many applications in machine learning for psychometrics, chemometrics, signal processing, and computer vision, including clustering, dimensionality reduction, and latent factor models (16). Moreover, tensor factorization-based methods have been proposed for the imputation and compression of traffic data collected from stationary and mobile sensors (17–20). These studies focus on the spatial dimension of link-based flow or speed and the temporal dimensions of steps and periods. Nonetheless, they do not address the interplay between different spatial locations. Compared with the one-dimensional spatial link, the data complexity of O-D matrices increases with the spatial contents. Thus, we can model collective mobility as a three-way (origin  $\times$  destination  $\times$  time) tensor. Although performing tensor decomposition (TD) in O-D matrices is not new, this work contributes to the state of the art with its application to high-dimensional trip data over various periods to reveal valuable insights into spatiotemporal interactions. The objective is to find spatial clusters, temporal patterns, and the correlation of these two aspects for mobile phone data observed in the province of Liège, Belgium. In the experiment, we defined mobile phone cells as traffic analysis zones and applied the hourly mean number of trips accumulated over a regular week and a holiday week to discuss travel patterns on weekdays and weekends. The intention is to seek the underlying trip purpose as well.

The rest of the paper is organized as follows. We first discuss multidimensional TD-related works in traffic analysis. Then, in the Methods section, we describe the mobile phone data and the TD model. In the Results section, we present the context for the choice of the TD model and the findings of spatial clusters and temporal patterns. Insights into mobility structure are drawn in

the Discussion section. Finally, we summarize limitations and future work in Section Conclusion.

## Related Work

Individual trajectories can be extracted from data collected by location-aware technologies (21). This promotes the study of the individual-based urban mobility model that allows scenario analysis related to human spatiotemporal behavior (22). Kuo et al. (23) pointed out that analyzing the immense amounts of individual-based data sets can be challenging beyond their volume. They proposed simplifying a data set of taxis' GPS traces into networks via coupled non-negative matrix factorization formulations. The intention was to view origin and destination information separately and co-cluster locations and times based on these views. O-D matrices and matrices containing time variant migrations (origin  $\times$  time and destination  $\times$  time) were built as two-dimensional matrices for the coupled matrix factorization to extract latent factors. Du et al. (24) applied tensor factorization to identify hot spots and summarize the corresponding traffic flow among them based on the public transit data. They simultaneously decomposed the O-D matrix and origin  $\times$  transfer  $\times$  destination (OTD) tensor into traffic flows among regions. To capture the variability in traveling patterns over time, they sliced the O-D and OTD data into several time slots.

Some researchers simultaneously model the spatial and temporal data using a high-dimensional tensor to discover the relationship between the spatial and temporal aspects. Fan et al. (7) adapted the non-negative tensor factorization and decomposed three-way (region  $\times$  timestamp  $\times$  day) tensors built from mobile sensing data (mobile phone users with GPS capacity) before and after the earthquake. To model the geographical shift of the "home" pattern, they co-factorized two people-flow tensors from different years in a unified framework. Wang et al. (15) applied mobile phone signaling data on the city scale for one week in morning and evening peak hours and summarized the trip records to a three-way tensor (origin  $\times$  destination  $\times$  time). They also compared the revealed spatial patterns with land use and population distribution. Sun and Axhausen (25) formulated the smart card data in a probabilistic setting and considered each record as a multivariate observation (time  $\times$  passenger type  $\times$  origin  $\times$  destination) sampled from an underlying distribution. The model is essentially equivalent to an NTD in which all vectors in factor matrices are replaced with a probability vector, and the core tensor is replaced with one that can also be regarded as a multi-way extension to the standard two-dimensional probabilistic latent semantic analysis. They

calculated the conditional probability across different modes in a small core tensor using Bayes' theorem to further quantify the latent interaction.

Wang et al. (26) modeled the time-evolving traffic networks into a three-order tensor (origin  $\times$  destination  $\times$  time) using a regularized NTD method. They considered taxi trajectory data and urban contextual knowledge together to discover the spatial clusters, temporal patterns, and relations among them. Zhu et al. (27) integrated Bayesian supervised learning into probabilistic tensor factorization to identify significant location-based socioeconomic variables and post-trip features and derive their probabilistic relationship between dynamic on-demand ride services (ridesharing, non-sharing, and taxi). The research team also developed a Bayesian clustering ensemble Gaussian process model to group stations with similar spatiotemporal patterns and fit the traffic volume for stations (28). Naveh and Kim (29) used non-negative TD to extract traveler movement patterns from large-scale smart card systems and roadside Bluetooth detectors. They focused on the in-depth analyses of day-of-week variations in three graph types and the differences between public transport and road traffic mobility patterns. Ghosal (30) predicted the travel time of a given path using GPS trajectories from vehicles by optimizing the TD. Since the three-dimensional tensor (segments  $\times$  drivers  $\times$  time) was very sparse, the author collaboratively decomposed the tensor with two matrices containing features of the road segment and correlation between different time slots with regard to the coarse-grained traffic conditions.

The existing works prove the efficiency of TD methods inferring spatial patterns of people's movements based on various emerging data sources. Meanwhile, we observe two main challenges and problems. First, distinct researchers find different patterns as they use diverse data sources. For instance, clear differences exist between mobility patterns across different days and transport modes. Moreover, time-of-day temporal profiles of trip demand aggregated over space are dissimilar between weekdays and weekends (29). Sun and Axhausen (25) found that public transit journeys demonstrate strong bidirectional homogeneity as a result of the regular home-based trips. However, Du et al. (24) showed that the O-D and D-O patterns are highly similar when using all-day passenger records to analyze movement and behaviors, while the similarity in flows reduces substantially when specific morning and evening peak hours are considered. Second, the TD model requires domain knowledge for result interpretation. The issue of selecting an appropriate algorithm to determine key elements, such as the core sensor size in TD models, is crucial, and it may further influence the interpretability of the final results. To meet the challenge above and fill the research gap, in this

paper, we analyzed a large-scale mobile phone-based mobility network across urban and rural areas on different days, in regular and holiday weeks. In addition, we tested different algorithms for the NTD considering the algorithm processing time and the reconstruction mean squared error. The focus of this study is on gaining new empirical insight using different data sources rather than contributing to data mining technologies.

## Methods

### Data Sets

Aggregated mobile phone data from the province of Liège were provided by the regional government (SPW Mobilité et Infrastructures) in the form of 336 (7 days  $\times$  24 h  $\times$  2 periods) hourly mean O-D matrices. The two periods for which the hourly means were tabulated concern regular weeks (from January 15, 2018 to February 8, 2018) and holiday weeks (the Carnival and Easter holiday weeks from February 23, 2018 to March 18, 2018).

To provide the aggregate O-D matrices, the province of Liège has been split into 310 zones (Figure 1 given by SPW) representing the unions of polygons built from the Voronoi diagram. The black delineations in Figure 1 show 84 municipalities in the province of Liège, and the colored ones represent mobile phone cells.

Note that privacy legislation means we were only provided with the aggregate O-D matrices. Thus, we do not have access to the raw mobile phone data in which individuals' information would reveal the underlying trips. Notwithstanding, we can compare the mobile phone-based origins and destinations with locations described by STATBEL (the Belgian Statistical Office). To check how closely they match, we looked into STATBEL's NIS coding system, which assigns a numeric code to each administrative unit to facilitate the production of georeferenced statistics. There are 270 out of 310 mobile phone zones that have the same NSI6 codes as STATBEL's sub-communes, and at least 80% of the given mobile phone cells' locations are less than 250 m (Euclidean distance) away from the STATBEL NSI6-zone centroids. However, when we spatially aggregated the 310 mobile phone zones back to the municipality level, we made a comparable visualization with 84 municipalities (NSI5) from STATBEL (Figure 2). We computed the spatial intersection ratios of Figure 2. The result shows that around 75% of zone pairs have at least 70% spatial matches. A more elaborate discussion of the comparison can be found in Gong et al. (31).

As mentioned above, a distinction is made between regular and holiday trips. After all, public holidays have a significant impact on travel patterns (32, 33). Based on the 336 (7 days  $\times$  24 h  $\times$  2 periods) hourly O-D

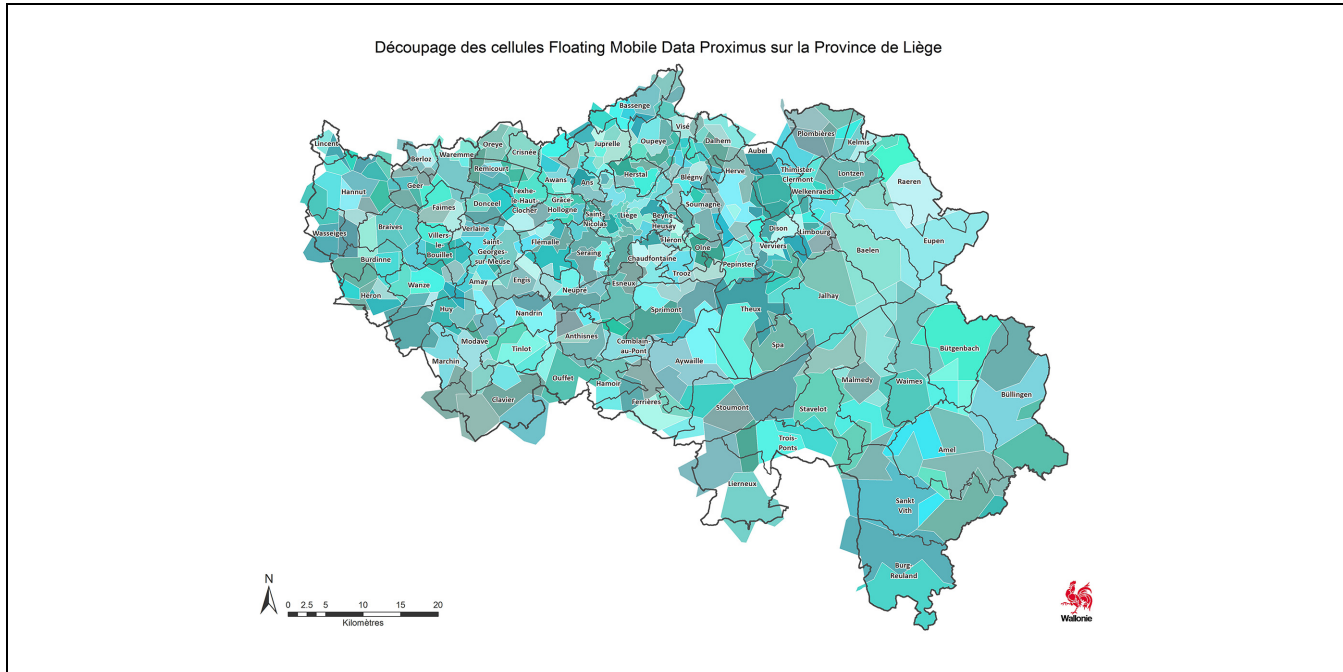


Figure 1. Delineation of floating mobile data proximus cells in the province of Liège.

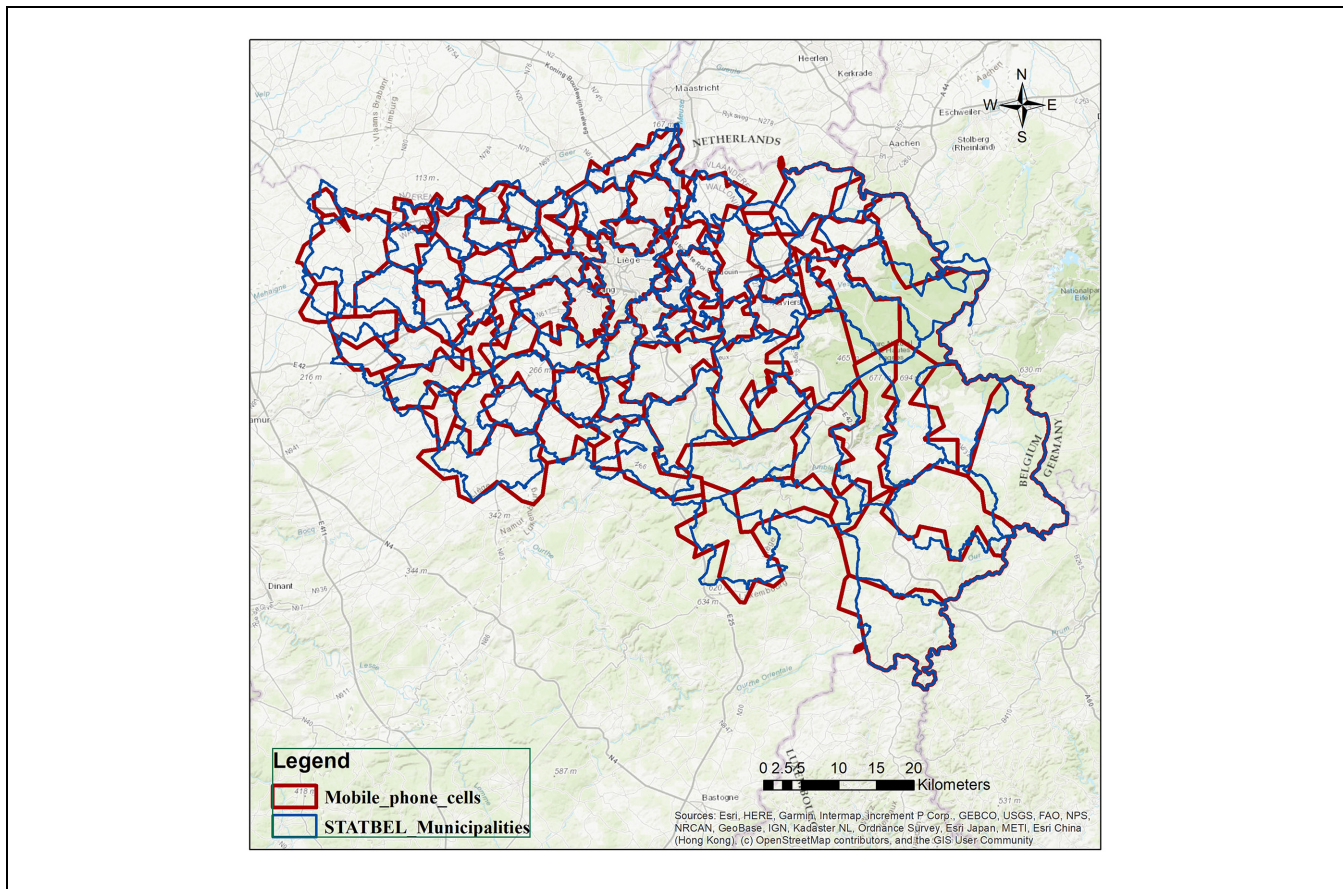
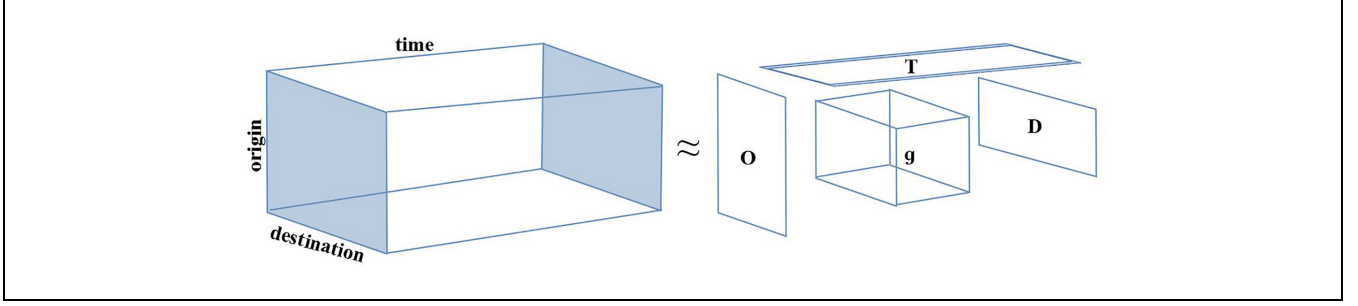


Figure 2. Mobile phone cells compared with STATBEL (Belgian statistical office) zones at the municipality level.



**Figure 3.** Tucker decomposition of the three-order.

matrices, we derived an average of 1.9 trips per day per inhabitant in the province of Liège. According to the last web-based national mobility survey in 2016 (MONITOR), Belgians make an average of 2.2 trips per day, which is comparable with the average trip rate derived from mobile phone-based O-D matrices for the province of Liège.

To filter out repetitive patterns, we reprocessed the 336 hourly O-D matrices and computed the averages for four types of day: regular weekdays, regular weekend days, holiday weekdays, and holiday weekend days, thus reducing the number of hourly O-D matrices to 96 (4 types of days  $\times$  24h) hourly O-D matrices. Since we focus on the province of Liège, the O-D trips whose origins or destinations are not inside the research area have been filtered out.

### Tucker Decomposition

The objective is to understand how different areas' populations move with the changing times. Since the mobile phone data consists of hourly mean O-D trips, we can manage the data as a third-order tensor with three modes: origin, destination, and time. A tensor is a multi-dimensional array whose decomposition has been applied to data arrays for decades to extract and explain their properties (34). A vector is a 1-order tensor, a matrix is a 2-order tensor, a cube is a 3-order tensor, and so on (35). According to Kolda and Bader (34), the Tucker decomposition is a form of higher-order principal component analysis (PCA), which decomposes a tensor into a core tensor multiplied (or transformed) by a matrix along each mode. The philosophy of such algorithms is to approximate the tensor through a linear combination of a few basic tensors (rank 1) under certain constraints (7, 35). The core tensor derived from Tucker decomposition shows the level of interaction between the different modes. Therefore, we chose Tucker TD to find the hidden patterns of traffic analysis zones and time. In this study, the mobile phone-based O-D matrices are denoted as a three-order tensor  $\mathcal{X} \in \mathcal{R}^{I \times J \times K}$ , whose  $(i, j, k)$ -th

entry  $x_{ijk}$  represents the traffic volume from origin  $i$  to destination  $j$  in time domain  $k$ . The Tucker decomposition in (Figure 3) is:

$$\mathcal{X} \approx \mathcal{G} \times_1 \mathcal{O} \times_2 \mathcal{D} \times_3 \mathcal{T} = \sum_{m=1}^M \sum_{n=1}^N \sum_{p=1}^P g_{mnp} o_m \circ d_n \circ t_p \quad (1)$$

In Equation 1,  $\times_1$  represents the tensor-matrix multiplication on mode-1. If  $M, N, P$  are smaller than  $I, J, K$ , the core tensor  $\mathcal{G} \in \mathcal{R}^{M \times N \times P}$  can be thought of as a compressed version of  $\mathcal{X}$ , while  $\mathcal{O} \in \mathcal{R}^{I \times M}$ ,  $\mathcal{D} \in \mathcal{R}^{J \times N}$ ,  $\mathcal{T} \in \mathcal{R}^{K \times P}$ , are factor matrices and can be considered as the principal components in each mode (34). The notation  $\circ$  describes the outer product, where  $\mathbf{o} \circ \mathbf{d} = \mathbf{od}^T$ , and  $o_m, d_n, t_p$  represent the  $m$ th,  $n$ th,  $p$ th column vector of the mode matrices  $\mathcal{O}, \mathcal{D}, \mathcal{T}$ , respectively (35). Considering O-D trips are over-dispersed count data, we proposed the non-negative Tucker decomposition (NTD) to derive spatial clusters and temporal patterns (26). Moreover, the log function (Equation 2) is applied for the tensor scaling to reduce the impact of high value.

$$\hat{x}_{ijk} = \log_2(1 + x_{ijk}) \quad (2)$$

Given the observed tensor  $\hat{\mathcal{X}}$ , we can obtain an exact Tucker decomposition of rank  $(R_1, R_2, R_3)$ , where  $R_n = \text{rank}_n(\hat{\mathcal{X}})$ , by solving the following optimization problem:

$$\min_{\mathcal{G}, \mathcal{O}, \mathcal{D}, \mathcal{T}} \|\hat{\mathcal{X}} - \mathcal{G} \times_1 \mathcal{O} \times_2 \mathcal{D} \times_3 \mathcal{T}\|_F^2 \quad (3)$$

In this objective error function,  $\|\cdot\|_F^2$  denotes the Frobenius norm, and it numerically equals the square root of the sum of squares for all elements. It returns the norm of the tensor based on the Euclidean distance (7). Numerous software libraries have been developed for tensor computation. This work adopted the open-source TensorLy library (36) to implement NTD. There are two algorithms available in TensorLy to compute NTD: i)

multiplicative updates (MU); and ii) non-negative alternating least squares (ALS) using Hierarchical ALS (HALS).

The MU algorithms iteratively matricize tensor into each mode. Matricizing a tensor is analogous to vectorizing a matrix. For MU in Tucker decomposition, we typically use alternating optimization, updating one factor matrix at a time while keeping the others fixed. Assuming the factor matrices  $\mathcal{O}, \mathcal{D}, \mathcal{T}$  as  $\mathcal{A}_n$ , the mode- $n$  matricization of  $\mathcal{X}$  in Equation 1 can be expressed by Kronecker products ( $\otimes$ ) of the mode- $n$  matricization of the core tensor and factor matrix (35), given by:

$$\mathcal{X}_{-n} \approx \mathcal{A}_n \mathcal{G}_n (\mathcal{A}_{-n})^T \quad (4)$$

$$\mathcal{A}_{-n} = [\mathcal{A}_N \otimes \dots \otimes \mathcal{A}_{n+1} \otimes \mathcal{A}_{n-1} \otimes \dots \otimes \mathcal{A}_1] \quad (5)$$

Here,  $N = 3$  is the number of tensor orders. If we denote  $\mathcal{X}^k$  as the approximation to  $\mathcal{X}$  at the  $k$ th iteration, and  $\mathcal{X}_{-n}^k$  as the approximation to  $\mathcal{X}$  at the  $k$ th iteration with the  $n$ th factor matrix excluded, the update equation of mode-1 (origin) for MU in NTD is as follows:

$$\mathcal{A}_1^{k+1} = \mathcal{A}_1^k * \left( \frac{\mathcal{X} \times_1 (\mathcal{A}_2^k)^T \times_2 (\mathcal{A}_3^k)^T}{\mathcal{G}^k \times_1 \mathcal{A}_1^k \times_2 \mathcal{A}_2^k \times_3 \mathcal{A}_3^k} \right) \quad (6)$$

where  $*$  is the Hadamard product, also known as the element-wise product. The numerator term captures how well the current estimate of the tensor matches the original tensor while keeping the other factor matrices fixed. The denominator term reconstructs the tensor using current estimates of all factor matrices except mode-1 and the current estimate of the core tensor to ensure normalization and stability. Similarly, we can update mode-2 and mode-3 by cyclically fixing each one and updating the rest. After updating the mode matrix, we can update the core tensor using the following equation:

$$\mathcal{G}^{k+1} = \mathcal{G}^k * \left( \frac{\mathcal{X} \times_1 (\mathcal{A}_1^{k+1})^T \times_2 (\mathcal{A}_2^{k+1})^T \times_3 (\mathcal{A}_3^{k+1})^T}{\mathcal{G}^k \times_1 (\mathcal{A}_1^{k+1})^T \mathcal{A}_1^{k+1} \times_2 (\mathcal{A}_2^{k+1})^T \mathcal{A}_2^{k+1} \times_3 (\mathcal{A}_3^{k+1})^T \mathcal{A}_3^{k+1}} \right) \quad (7)$$

In Equation 7, the numerator term represents how well the current estimate of the tensor matches the original tensor when the core tensor is updated, while keeping all factor matrices fixed. The denominator term reconstructs the tensor using the current estimates of all factor matrices and the core tensor.

Non-negative ALS is another iterative optimization algorithm commonly used for Tucker decomposition (15). By alternatively improving one matrix while keeping other matrices fixed, we can obtain the following non-negative ALS update rule for  $\mathcal{A}_n$  and  $\mathcal{G}$ :

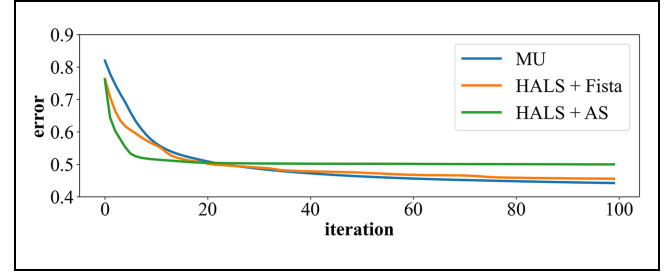


**Figure 4.** Comparison of error per iteration of NTD algorithms in TensorLy.

Note: NTD = non-negative Tucker decomposition; mu = multiplicative updates; HALS = hierarchical alternating least squares; AS = active set; FISTA = fast iterative shrinkage thresholding algorithm.

$$\mathcal{A}_1^{k+1} = \arg \min_{\mathcal{A}_1 \geq 0} \|\mathcal{X} - (\mathcal{G}^k \times_1 \mathcal{A}_1 \times_2 \mathcal{A}_2^k \times_3 \mathcal{A}_3^k)\|_F^2 \quad (8)$$

$$\mathcal{G}^{k+1} = \arg \min_{\mathcal{G} \geq 0} \|\mathcal{X} - (\mathcal{G} \times_1 \mathcal{A}_1^{k+1} \times_2 \mathcal{A}_2^{k+1} \times_3 \mathcal{A}_3^{k+1})\|_F^2 \quad (9)$$

Each update involves solving a least squares problem with non-negativity constraints until convergence. Within the TensorLy package, HALS can be combined with two different algorithms to update the core and factors: active set (AS) and fast iterative shrinkage thresholding algorithm (FISTA).

To seek the best choice of NTD in TensorLy for our data, considering the algorithm processing time and reconstruction mean squared error, we tested MU, HALS + FISTA, and HALS + AS with one regular weekday O-D matrices by fixing the same rank values (45,45,24), using the default singular value decomposition (SVD) as initialization strategies and a maximum of 100 iterations. As a result, MU is better than the HALS with

both FISTA and AS, considering the convergence error (Figure 4). HALS + AS tends to converge faster than MU. However, its computational time is much higher than MU. Both MU and HALS have their strengths and weaknesses. The impact factors, such as the size of the data, computational resources available, and specific characteristics of the problem at hand, may affect the choice between these two methods. We chose the method with the minimal reconstruction error as our first priority. Therefore, we applied MU for NTD in the following analysis. Four data sets corresponding to the four types of days mentioned

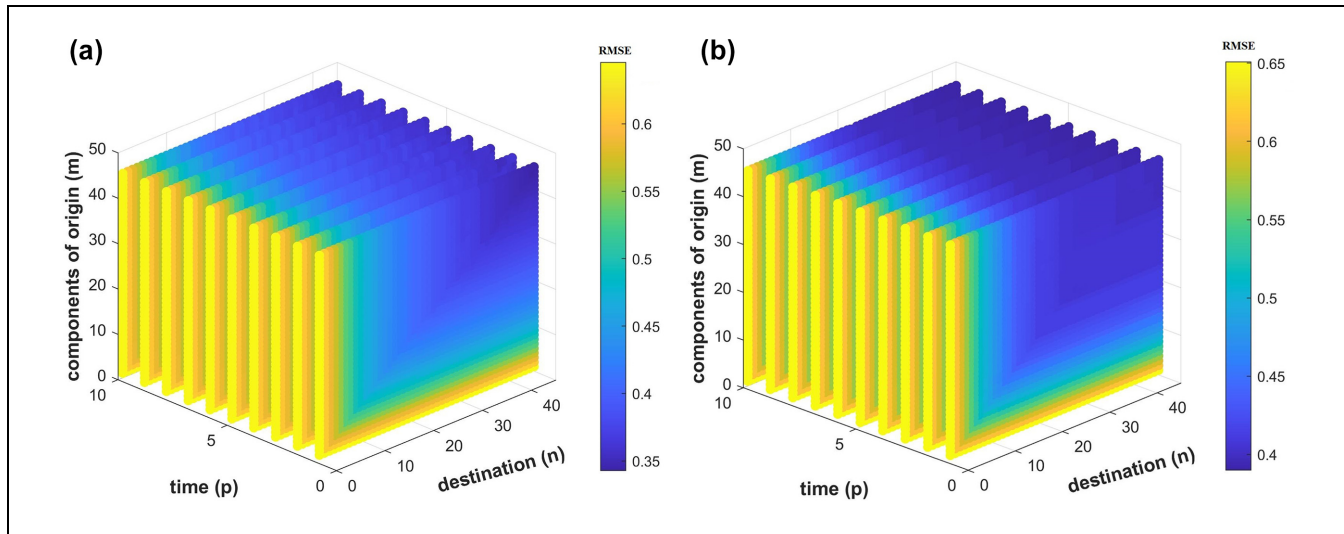


**Figure 5.** Reconstruction root mean squared error (RMSE) for tensors by tuning  $m, n, p$ : (a) one regular weekday; (b) one holiday weekday.

above are built as four  $(310 \times 310 \times 24)$  input traffic tensors. The original tensor has size  $310^2 \times 24$ , whereas after rank- $R$  decomposition, the dimensionality is reduced to  $R_1 \times 310 + R_2 \times 310 + R_3 \times 24$  (29).

## Results

### The Rank of Hidden Space and Time

This experiment aims to find the spatial clusters and temporal patterns, and the correlation between them based on the time-evolving O-D trips. The outputs of NTD include: 1) origin-decomposed factors; 2) destination-decomposed factors; 3) time-decomposed factors; and 4) the core tensor that contains the spatial and temporal correlation. From 1) and 2), we can ascertain to which cluster a traffic analysis zone belongs. Moreover, it is possible to find temporal patterns, such as the morning peak indicated by time-decomposed factors. Therefore, the first step is to find rank values  $(m, n, p)$  showing latent components for **origin**, **destination**, and **time**, respectively. We conducted experiments with the potential rank values  $m$  and  $n$  ranging from 1 to 50 and  $p$  ranging from 1 to 10 on four tensors. Each NTD with the unique rank  $(m, n, p)$  setting runs a maximum of 40 iterations based on Figure 4. Secondly, to evaluate the choice of rank  $(m, n, p)$ , we computed the output tensor from the decomposed factors and compared the root mean squared error (RMSE) between the reconstructed and the observed tensor. By changing the spatial and temporal components' number, we derived the reconstruction RMSE 3-D plots for one regular weekday and one holiday weekday Figure 5).

In the existing research (15, 25, 26), decomposed clusters for origins and destinations are usually set as the same, assuming they are balanced. We have discussed the possible dissimilarity of origins-destinations caused by different data inputs and temporal profiles in Section Related Work. In this study, the evaluation of the rank  $(m, n, p)$  choice shows that: 1) the O-D and D-O patterns have high similarity using all-day mobile phone records to analyze movements behavior; and 2) the hourly mean temporal variability in people flow over the day does not have a significant influence on the final determination of the number of spatial clusters. To better depict the convergence in the spatial and temporal mode, we fixed one parameter type and tuned the other in different iterations of NTD. As we have a maximum of 24h within a day and 310 zones, the maximum spatial and temporal components of NTD are 310 and 24. In addition, the origin and destination have similarities based on Figure 5. Therefore, we chose the same rank for  $m$  and  $n$ .

We looked into 2-D RMSE line plots for adjusting the spatial rank with  $p = 3$  and the temporal rank with  $m$  and  $n = 40$ . The results are depicted in Figure 6, from which we learned that: 1) RMSE results obtained using four tensors are all convergent at the turn of 40 components for spatial patterns; 2) the variance in RMSE for temporal patterns is relatively small compared with the spatial one; and 3) RMSE of time does not seem to be convergent, especially for the holiday weekday and the regular weekend. Still, we can find the convergence for the regular weekday, and many components leads to a higher RMSE than the situation when  $p = 3$ . The difference in temporal patterns between days indicates that it makes sense to differentiate people's travel patterns

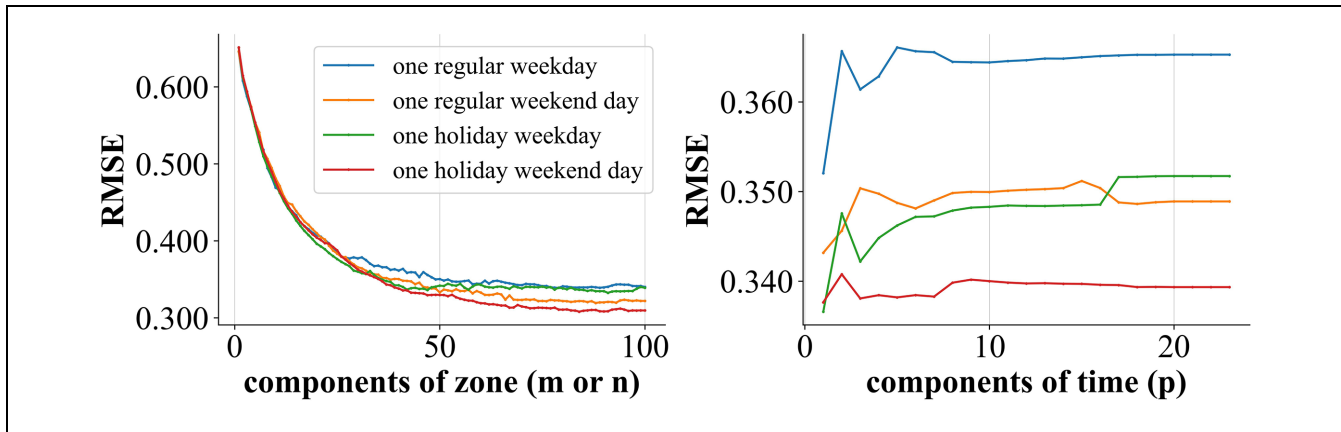


**Figure 6.** Reconstruction root mean squared error (RMSE) by fixing: (a)  $p = 3$ ; and (b) spatial rank  $(m, n) = 40$ .

between weekdays and weekends. In the following discussion, we chose  $m$  and  $n = 40$  and  $p = 3$  as latent spatial and temporal dimensions and tried to visualize the interaction between spatial clusters and temporal patterns geographically and to draw insights into human motion in the province of Liège.

### Insights of Temporal Patterns and Spatial Clusters

**Temporal Patterns.** Some scientists, such as Peng et al. (37), have categorized the trip purpose into three basic patterns, taking a typical workday as an example: home to the workplace in the early morning; workplaces to workplaces in the daytime; and workplaces to home or other places at dusk. Our temporal decomposition results on the regular weekday fits this well-known finding. Moreover, we included the discussion on typical weekends and holiday weekdays to extract latent factors. NTD belongs to the family of matrix/tensor factorization algorithms approximating the matrix/tensor through a linear combination of a few basic tensors (7). Therefore, a people flow can be approximated by a linear combination of basis flows such as commuting and other working patterns (37). The coefficients in the linear combination indicating the strength of each basis flow are factor matrices derived from our NTD analysis.

With regard to the temporal latent factors, each hour's factor represents the strength of the people flow during this hour. We first assumed that all four O-D tensors have three temporal clusters and depicted factors of time (Figure 7). The results reveal that the temporal patterns observed during regular weekdays can be categorized under three distinct, purpose-based categories: cluster C1 in Figure 7 can be interpreted as the pattern of workplaces to workplaces during the daytime; cluster C2 with the evening peak is the workplaces-to-home pattern; and cluster C3 with the morning peak is the home-to-

workplaces pattern. Secondly, the analysis indicates that weekdays classified as holidays exhibit the same three-group categorization as regular weekdays. However, for clusters characterized by morning and evening activity peaks, the flow intensity is diminished compared with that observed on a typical weekday. Finally, on weekends, the cluster characterized by a morning peak disappears, suggesting the optimal categorization into two clusters rather than three. This observation aligns with the findings presented in Figure 6. In the given mobile phone-based O-D matrices, the number of trips from 0:00 to 4:00 a.m. is aggregated as one value. For instance, the mean O-D trips of hour 5 in the morning represent the accumulated number of trips from 5:00 to 6:00 a.m. To make complete 24-h O-D tensors, we took an average of the total trip value from 0:00 to 4:00 a.m. as the first five hourly mean O-D trips. Thus, we see the same first five-factor values in each line plot in Figure 7.

As mentioned above, analyzing the weekday's temporal patterns reveals the morning and evening peaks, and the daytime traffic situation. The morning peak is reached around 7:00 to 8:00 a.m. and the evening peak around 4:00 to 5:00 p.m. during regular and holiday weekdays. However, the patterns show that the morning and evening peaks on regular weekdays are higher than those on holiday weekdays, which is understandable as some people will be away from the office for vacation during holiday weekdays. Compared with the weekday's temporal patterns, the morning peak on the weekend day disappears. In contrast, the factors drop after 4:00 to 5:00 a.m. on the regular weekend, possibly caused by the end of night-life events. There are not many differences in temporal patterns between the regular weekend and holiday weekend apart from the factors of the evening peak around 4:00 to 6:00 p.m. on the regular weekend being much higher than on the holiday weekend, which possibly represents a higher number of trips going home



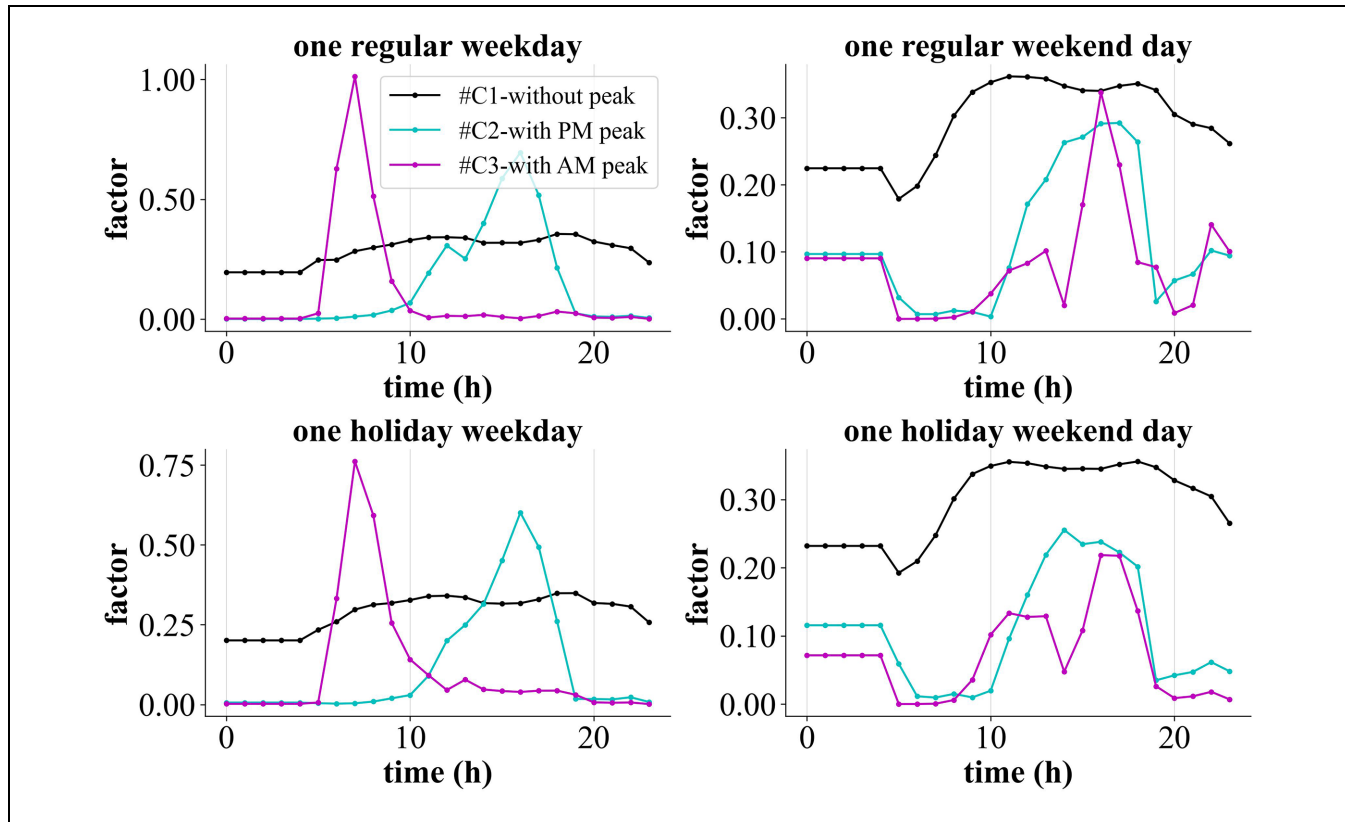


**Figure 7.** Temporal patterns for four data sets.

or joining night-event. The possible reason for this is the increased relaxing time during holiday weekdays rather than regular weekdays. Therefore, people tend to reduce the demand for traveling at the weekend during the holiday weeks. In summary, Figure 7 can give us intuitional guidance on the temporal management of urban mobility patterns for regular and holiday weeks. The following subsection will present the correlation of temporal patterns with spatial characteristics.

**Trip Generation and Attraction Patterns.** Each mobile phone cell represents not only an origin but also a destination. From the mode-1 and mode-2 decomposed factors of Tucker decomposition, we can learn the spatial clusters based on origin and destination perspectives. As discussed above, the outputs of the mode-1 factorization and mode-2 factorization in Equation 1 are two  $310 \times 40$ -factor arrays. Each factor value is the coefficient of the linear combination of spatial patterns and indicates the strength of the basis flow. If we normalize factor values for each traffic analysis zone (TAZ), we can show to what extent the TAZ can be categorized as one of the 40 clusters. For simplicity and efficiency, the cluster is chosen for each TAZ based on the highest factor value.

Despite choosing the same number of clusters for origin and destination in NTD, some clusters may be empty (without any mobile phone cell assigned) purely based on the maximum factor value. This means the spatial cluster number is predefined as 40, but the truly found origin- or destination-based clusters can be less than 40. The shape of each cluster can be different, which makes sense as the distribution of origin-based factor values is similar to the destination-based. Still, the values presenting the flow strength are not exactly the same. This is also one aspect of the imbalance between attraction and production. However, this imbalance is not significant on the province scale, using the 24-h O-D matrices. Figure 8 shows the origin- and destination-based spatial clusterings on a regular weekday. Results indicate that spatial clusters of origins or destinations are geographically close, which is in line with the results of Wang et al. (26). Dissimilarity happens especially in the area (around cluster 1) with a denser population in the north (see the population distribution map in the Appendix Figure A-1).

In our study, around 80% of TAZs are categorized in the same group, comparing results of the origin clustering with the destination clustering on the regular weekday, and the similarity increases to more than 90% at the weekend and on the holiday weekday. We have

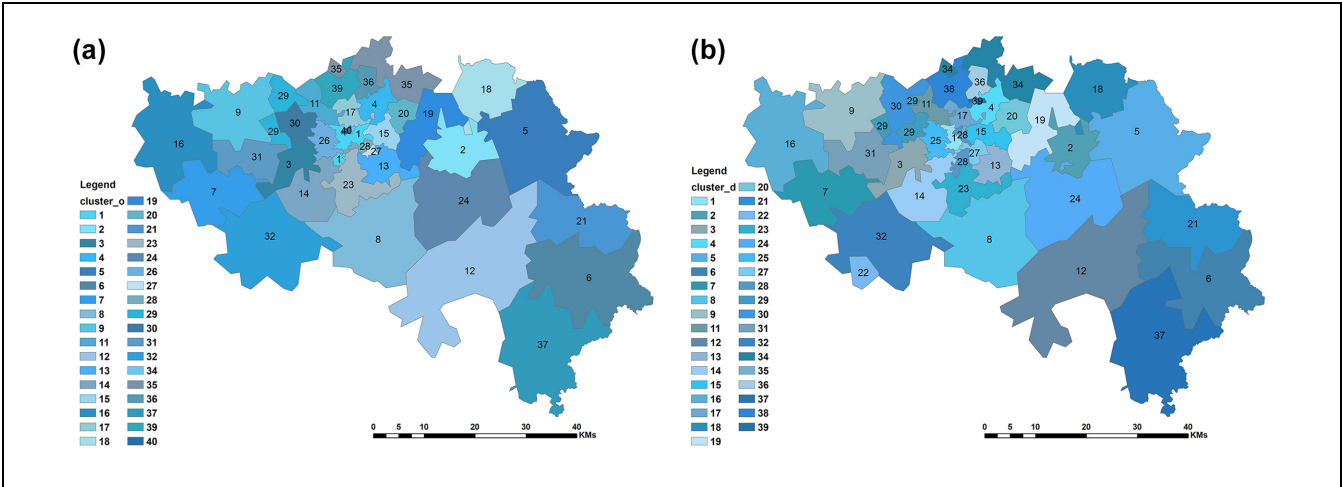


**Figure 8.** Results of the spatial clustering on a regular weekday: (a) clusters of origins on a regular weekday; and (b) clusters of destinations on a regular weekday.

presented the reason behind this in the rank analysis subsection. However, the dissimilarity in spatial clustering between origins and destinations among different types of day increases. For instance, the distribution of origin clusters on the weekday is different from the distribution of origin clusters at the weekend (see Appendix Figure A-2), and only about 35% of mobile phone cells are assigned to the same origin cluster. The results imply the difference in human motion between weekdays and weekends.

From Equation 1, it is noted that each column of  $\mathcal{O}$  interacts with every column of  $\mathcal{D}$  and every column of  $\mathcal{T}$ , and the strength of this interaction is encoded in the corresponding elements of  $\mathcal{G}$  (16). Therefore, an individual element of the core tensor serves as the weight of the associated combination of  $\mathcal{O}$ ,  $\mathcal{D}$ ,  $\mathcal{T}$  (35). The visualization of this weight could help reveal the underlying “essential” interactions between triples of columns of  $\mathcal{O}$ ,  $\mathcal{D}$ ,  $\mathcal{T}$ . We took the compressed core tensor  $\mathcal{G}$  ( $40 \times 40 \times 3$ ) from the regular weekday as the example to further infer the relationship between spatial and temporal patterns. Figure 9 depicts the interaction weights between 40 origin clusters (Y-axis in the heatmap) and 40 destination clusters (X-axis in the heatmap) for three temporal patterns extracted from the core tensor. The figures show that the intensity of within-cluster interactions during the daytime (Figure 9b) is much higher than the other two temporal patterns. As our NTD mostly combines neighboring zones into larger clusters, the result of more within-cluster trips than inter-cluster trips implies that there are more short-distance trips than long-distance trips. Furthermore, we can find the symmetry of O-D spatial interactions between the morning peak (Figure 9a) and the afternoon peak (Figure 9c). Apart from the symmetry, we can see, for instance, clusters 1 and 28 attract

more trips than other clusters during the morning peak, whereas they generate more trips than other clusters during the afternoon peak.

Next, we evaluated the NTD results for temporal patterns with the morning and evening peaks on a regular weekday by introducing the population distribution and the commuting matrix. The mobile phone data were collected at the beginning of 2018; thus, we selected the 2016 Belgium population according to the  $km^2$  grid and the commuting matrix from the 2011 Census. In the data subsection, we have described the difference between the delineation of mobile phone cells and the national geo-referenced statistics. Approximations of population and number of commutes for each cell were performed and compared with the reconstructed flow for the morning and afternoon periods separately. More details can be seen in the Appendix Figure A-3. Based on Figure 7, we chose two sliced tensors from 5:00 to 10:00 a.m. and 13:00 to 19:00 p.m. as inputs for NTD with rank ( $40 \times 40 \times 1$ ). We were interested in the inbound trips for two peaks, so we rebuilt the arrivals and accumulated trips for each destination and cluster. After that, the Person correlation coefficients were computed, indicating a strong positive relationship between population and inbound trips Table 1. The number of commutes also positively correlates with inbound trips; however, the correlation decreases in the afternoon.

Lastly, we investigated the interaction weights between spatial patterns in the same temporal domain. Weights within clusters are much higher than inter-clusters and unsuitable for spatial depictions. Therefore, we sorted clusters based on the total inbound trips, excluding the intra-cluster trips, to check which clusters have higher interaction. The first two clusters found were selected as

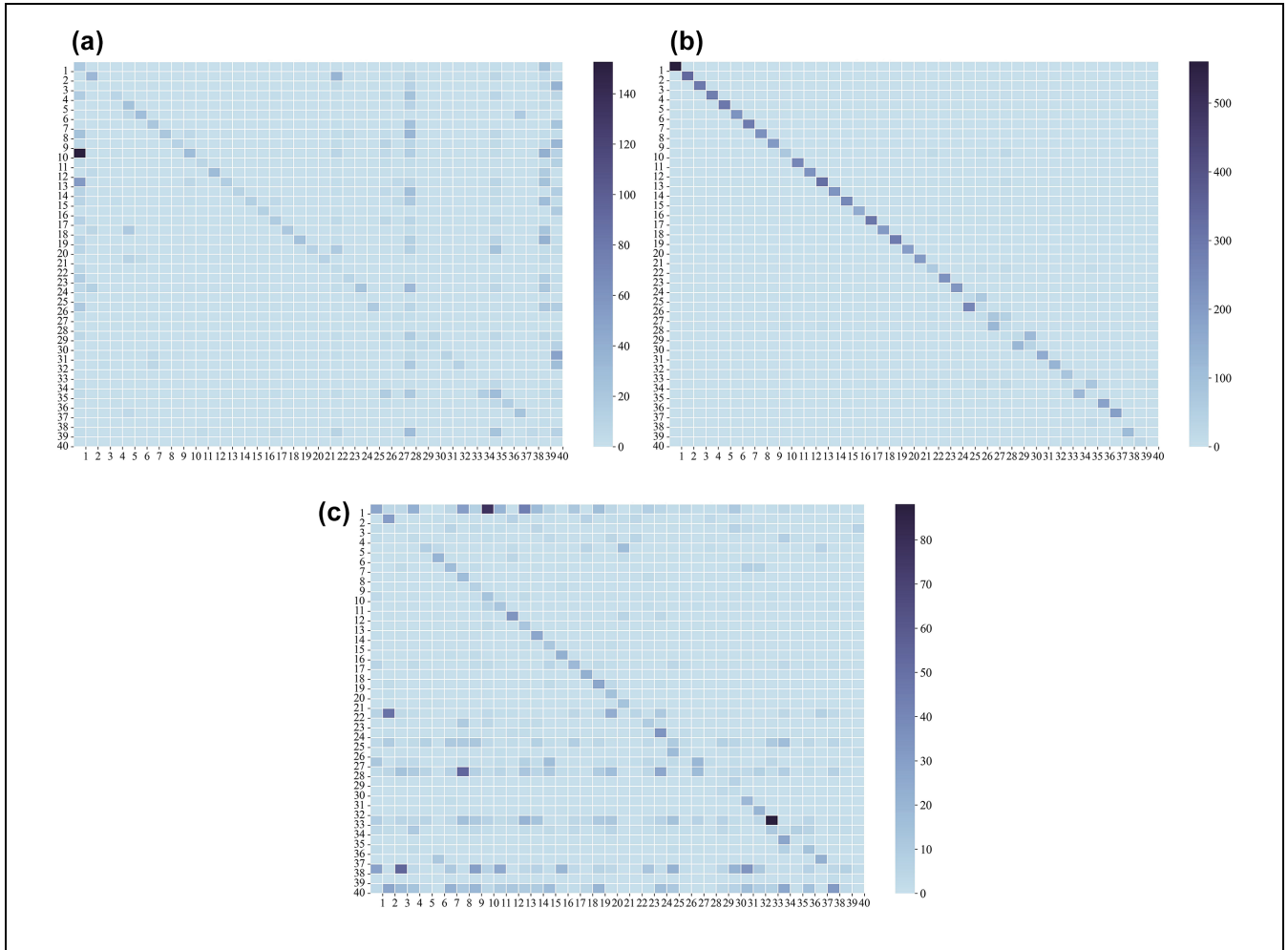


**Figure 9.** Weights of interactions between spatial clusters and temporal patterns: (a) spatial interactions for temporal patterns with the morning peak; (b) spatial interactions for temporal patterns during daytime; and (c) spatial interactions for temporal patterns with the evening peak.

**Table 1.** The Pearson Correlation Coefficient Between Reconstructed Flow and Other Observations Including Commuting Matrix and Population Distribution

Reconstructed flow	Morning period coefficient	5:00 to 10:00 a.m. <i>p</i> -value
Number of commuting at TAZ level	0.814	≤ 0.0001
Number of population at TAZ level	0.805	≤ 0.0001
Number of population at cluster level	0.893	≤ 0.0001
	Evening peak	13:00 to 19:00 p.m.
Number of commuting at TAZ level	0.675	≤ 0.0001
Number of population at TAZ level	0.858	≤ 0.0001
Number of population at cluster level	0.904	≤ 0.0001

Note: TAZ = traffic analysis zone.

representative of each temporal pattern; their connections were shown with the cluster where trips are generated. From Figure 10, we can see the shift of the attraction

center within a day in the research area. Additionally, this study provides insights into the intensity of human movement in relation to specific directions, which can assist

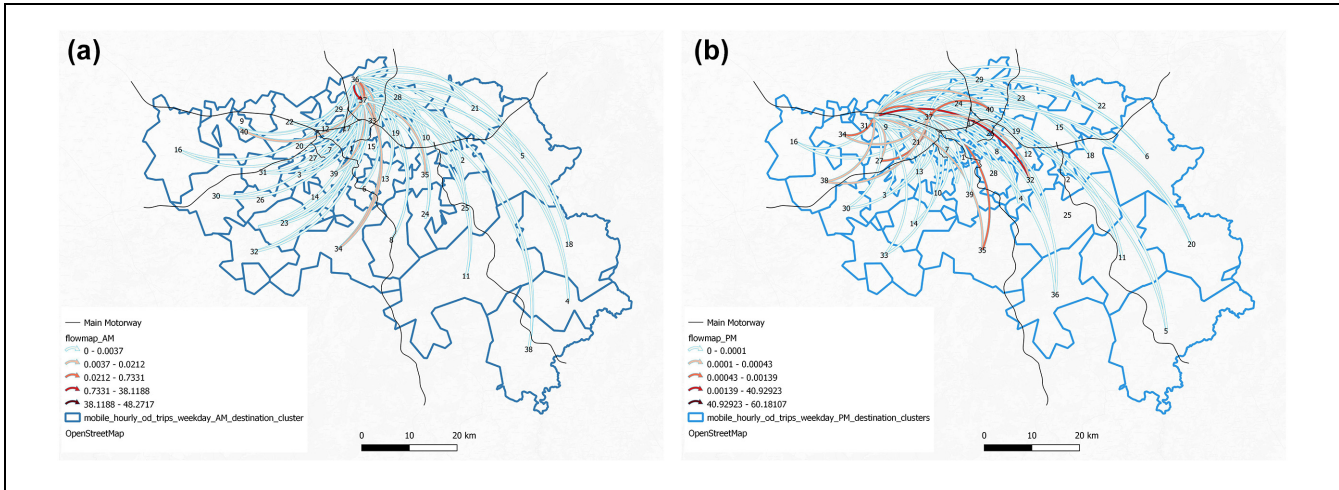


**Figure 10.** Results of the inter-clusters interaction on a regular weekday: (a) top two destination clusters in the morning; and (b) top two destination cluster in the afternoon.

city planners in formulating policies to manage urban environments better.

## Discussion

This study shows that non-negative Tucker decomposition can infer complex human mobility patterns based on mobile phone-based O-D matrices. The findings are consistent with the existing literature with regard to the origin and destination clustering and three temporal patterns on a typical weekday. However, we could not draw activity patterns for specific social groups with travel mode information since the data lack individual information. Still, this experiment shows the possibility of applying aggregated O-D matrices to reconstruct the travel demand and draw valuable insights into urban mobility patterns. First, we found the difference in mobility patterns between a working weekday and a weekend day.

Second, from the interaction of spatial clusters and the temporal pattern with the morning peak, we saw that places such as the Liège city center, offering more job opportunities, are attracting more trips than other places. Even though the O-D matrices do not contain any information about individuals or their trip purposes, the results of temporal patterns during the weekday are under the representation of three purpose-based categories, which can feed as activities for daily plan generation in the future.

Third, we can identify which residential areas generate more commuting trips to the central business district (CBD) of Liège. Comparing information on land use and the population distribution with spatial patterns identified by the TD, we can find that most of the central districts of spatial clusters are the TAZs with higher populations. The number of long-distance trips, such as

going to work or school, decreases for most places during the weekend, whereas nearby trips increase.

The findings mentioned above can support policy-makers in urban planning. However, we must clarify that the O-D matrices discussed here are only for the trips whose origins and destinations are both within the province of Liège. Trips originating from or arriving at a zone outside the province of Liège take around 16% of the total mobile phone-based O-D trips. Furthermore, given the relatively small size of Belgium and the specific location of the Liège province, cross-border trips, for instance, for commuting and shopping, are not captured either. Notwithstanding, as illustrated by Christmann et al. (38), these flows are non-negligible.

## Conclusions

This work focused on interpreting spatial clusters, temporal patterns, and the correlation between both by applying non-negative Tucker decomposition to mobile phone-based O-D matrices. The visualization proposed in this study explains how mobile phone data can be used to provide valuable information to citizens and authorities. The analysis indicates that 40 spatial clusters and three temporal patterns can be found based on the compression of O-D tensors. In addition, we should differentiate human motion on weekdays, weekends, regular weeks, and holidays.

NTD seems promising for analyzing mobility patterns. Meanwhile, we validated the reconstructed demand by introducing other comparable data sources. However, this study has limitations, as the provider of the mobile phone data has a limited market share, and we are not clear to what extent this can affect results.

Future research should focus on the reliability of estimated tensors. Moreover, we saw differences in spatial clustering with different data sets. Further research on evaluating the consistency and robustness of the clustering results is needed to delineate the approach's applicability clearly. Finally, an interesting future research direction would be to estimate the underlying trip purpose over different periods derived from NTD to generate daily activity plans.

### Acknowledgments

We thank Wallonia SPW Mobilité et Infrastructures for kindly providing the mobile phone data.

### Author Contributions

The authors confirm contribution to the paper as follows: study conception and design: Gong S; data collection: Gong S, and Teller J; analysis and interpretation of results: Gong S, Saadi I, Teller J, and Cools M; draft manuscript preparation: Gong S, and Cools M. All authors reviewed the results and approved the final version of the manuscript.




### Declaration of Conflicting Interests

The author(s) declared no potential conflicts of interest with respect to the research, authorship, and/or publication of this article.

### Funding

The author(s) disclosed receipt of the following financial support for the research, authorship, and/or publication of this article: This work has been funded through the Wal-e-Cities project, supported by the European Regional Development Fund (ERDF) and the Walloon Region of Belgium, and by the TrackGen project, supported by the Walloon Region of Belgium.

### ORCID iDs

Suxia Gong  <https://orcid.org/0000-0002-8468-8652>  
 Ismail Saadi  <https://orcid.org/0000-0002-3569-1003>  
 Mario Cools  <https://orcid.org/0000-0003-3098-2693>

### Data Accessibility Statement

The original contributions presented in the study are included in the article. Further inquiries can be directed to the corresponding author.

### Supplemental Material

Supplemental material for this article is available online.

### References

1. Caceres, N., J. P. Wideberg, and F. G. Benitez. Deriving Origin-Destination Data from a Mobile Phone Network. *IET Intelligent Transport Systems*, Vol. 1, No. 1, 2007, pp. 15–26.

2. Bonnel, P., M. Fekih, and Z. Smoreda. Origin-Destination Estimation Using Mobile Network Probe Data. *Transportation Research Procedia*, Vol. 32, 2018, pp. 69–81.
3. Calabrese, F., M. Colonna, P. Lovisolo, D. Parata, and C. Ratti. Real-Time Urban Monitoring Using Cell Phones: A Case Study in Rome. *IEEE Transactions on Intelligent Transportation Systems*, Vol. 12, No. 1, 2011, pp. 141–151.
4. Calabrese, F., M. Diao, G. Di Lorenzo, J. Ferreira, and C. Ratti. Understanding Individual Mobility Patterns from Urban Sensing Data: A Mobile Phone Trace Example. *Transportation Research Part C: Emerging Technologies*, Vol. 26, 2013, pp. 301–313.
5. Song, J., L. Zhang, Z. Qin, and M. A. Ramli. Spatiotemporal Evolving Patterns of Bike-Share Mobility Networks and Their Associations with Land-Use Conditions Before and After the COVID-19 Outbreak. *Physica A: Statistical Mechanics and its Applications*, Vol. 592, 2022, p. 126819.
6. Gibbs, H., Y. Liu, C. A. Pearson, C. I. Jarvis, C. Grundy, B. J. Quilty, C. Diamond, and R. M. Eggo. Changing Travel Patterns in China During the Early Stages of the COVID19 Pandemic. *Nature Communications*, Vol. 11, No. 1, 2020, pp. 1–9.
7. Fan, Z., X. Song, and R. Shibasaki. CitySpectrum: A Non-Negative Tensor Factorization Approach. *Proc., ACM International Joint Conference on Pervasive and Ubiquitous Computing, UbiComp 2014*, Seattle, WA, Association for Computing Machinery, New York, 2014, pp. 213–233.
8. Awad-Núñez, S., R. Julio, J. Gomez, B. Moya-Gómez, and J. S. González. Post-COVID-19 Travel Behaviour Patterns: Impact on the Willingness to Pay of Users of Public Transport and Shared Mobility Services in Spain. *European Transport Research Review*, Vol. 13, No. 1, 2021, pp. 1–18.
9. Ahas, R., A. Aasa, Y. Yuan, M. Raubal, Z. Smoreda, Y. Liu, C. Ziemlicki, M. Tiru, and M. Zook. Everyday Space–Time Geographies: Using Mobile Phone-Based Sensor Data to Monitor Urban Activity in Harbin, Paris, and Tallinn. *International Journal of Geographical Information Science*, Vol. 29, No. 11, 2015, pp. 2017–2039.
10. Anwar, T., C. Liu, H. L. Vu, M. S. Islam, and T. Sellis. Capturing the Spatiotemporal Evolution in Road Traffic Networks. *IEEE Transactions on Knowledge and Data Engineering*, Vol. 30, No. 8, 2018, pp. 1426–1439.
11. Yan, F., M. Zhang, and Z. Shi. Dynamic Partitioning of Urban Traffic Network Sub-Regions with Spatiotemporal Evolution of Traffic Flow. *Nonlinear Dynamics*, Vol. 105, No. 1, 2021, pp. 911–929.
12. Furtlehner, C., Y. Han, J.-M. Lasgouttes, V. Martin, F. Marchal, and F. Moutarde. Spatial and Temporal Analysis of Traffic States on Large Scale Networks. *Proc., 13th International IEEE Conference on Intelligent Transportation Systems*, Funchal, Portugal, IEEE, New York, 2010, pp. 1215–1220.
13. Sun, L., D. H. Lee, A. Erath, and X. Huang. Using Smart Card Data to Extract Passenger's Spatio-Temporal Density and Train's Trajectory of MRT System. *Proc., ACM SIGKDD International Conference on Knowledge Discovery*

- and Data Mining, Beijing, China, Association for Computing Machinery, New York, 2012, pp. 142–148.
14. Jiang, S., J. Ferreira, Jr., and M. C. Gonzalez. Discovering Urban Spatial-Temporal Structure from Human Activity Patterns. *Proc., ACM SIGKDD International Conference on Urban Computing*, Beijing, China, Association for Computing Machinery, New York, 2012, pp. 95–102.
  15. Wang, D., Z. Cai, Y. Cui, and X. M. Chen. Nonnegative Tensor Decomposition for Urban Mobility Analysis and Applications with Mobile Phone Data. *Transportmetrica A: Transport Science*, Vol. 18, No. 1, 2022, pp. 29–53.
  16. Sidiropoulos, N. D., L. De Lathauwer, X. Fu, K. Huang, E. E. Papalexakis, and C. Faloutsos. Tensor Decomposition for Signal Processing and Machine Learning. *IEEE Transactions on Signal Processing*, Vol. 65, No. 13, 2017, pp. 3551–3582.
  17. Asif, M. T., N. Mitrovic, J. Dauwels, and P. Jaillet. Matrix and Tensor Based Methods for Missing Data Estimation in Large Traffic Networks. *IEEE Transactions on Intelligent Transportation Systems*, Vol. 17, No. 7, 2016, pp. 1816–1825.
  18. Chen, X., Y. Chen, N. Saunier, and L. Sun. Scalable Low-Rank Tensor Learning for Spatiotemporal Traffic Data Imputation. *Transportation Research Part C: Emerging Technologies*, Vol. 129, 2021, p. 103226.
  19. Han, Y., and F. Moutarde. Analysis of Large-Scale Traffic Dynamics in an Urban Transportation Network Using Non-Negative Tensor Factorization. *International Journal of Intelligent Transportation Systems Research*, Vol. 14, No. 1, 2016, pp. 36–49.
  20. Tang, K., C. Tan, Y. Cao, J. Yao, and J. Sun. A Tensor Decomposition Method for Cycle-Based Traffic Volume Estimation Using Sampled Vehicle Trajectories. *Transportation Research Part C: Emerging Technologies*, Vol. 118, 2020, p. 102739.
  21. Schneider, C. M., V. Belik, T. Couronné, Z. Smoreda, and M. C. González. Unravelling Daily Human Mobility Motifs. *Journal of the Royal Society Interface*, Vol. 10, No. 84, 2013, p. 20130246.
  22. Xie, J., L. Yin, and L. Mao. A Modeling Framework for Individual-Based Urban Mobility Based on Data Fusion. *International Conference on Geoinformatics*, Vol. 2018, 2018, pp. 1–6.
  23. Kuo, C. T., J. Bailey, and I. Davidson. A Framework for Simplifying Trip Data into Networks via Coupled Matrix Factorization. *Proc., SIAM International Conference on Data Mining 2015, SDM 2015*, Society for Industrial and Applied Mathematics, Philadelphia, PA, 2015, pp. 739–747.
  24. Du, B., W. Zhou, C. Liu, Y. Cui, and H. Xiong. Transit Pattern Detection Using Tensor Factorization. *INFORMS Journal on Computing*, Vol. 31, No. 2, 2019, pp. 193–206.
  25. Sun, L., and K. W. Axhausen. Understanding Urban Mobility Patterns with a Probabilistic Tensor Factorization Framework. *Transportation Research Part B: Methodological*, Vol. 91, 2016, pp. 511–524.
  26. Wang, J., F. Gao, P. Cui, C. Li, and Z. Xiong. Discovering Urban Spatio-Temporal Structure from Time-Evolving Traffic Networks. *Proc., Asia-Pacific Web Conference*, Vol. 8709 LNCS, Changsha, China, Springer, Cham, 2014, pp. 93–104.
  27. Zhu, Z., L. Sun, X. Chen, and H. Yang. Integrating Probabilistic Tensor Factorization with Bayesian Supervised Learning for Dynamic Ridesharing Pattern Analysis. *Transportation Research Part C: Emerging Technologies*, Vol. 124, 2021, p. 102916.
  28. Zhu, Z., M. Xu, J. Ke, H. Yang, and X. M. Chen. A Bayesian Clustering Ensemble Gaussian Process Model for Network-Wide Traffic Flow Clustering and Prediction. *Transportation Research Part C: Emerging Technologies*, Vol. 148, 2023, p. 104032.
  29. Naveh, K. S., and J. Kim. Urban Trajectory Analytics: Day-of-Week Movement Pattern Mining Using Tensor Factorization. *IEEE Transactions on Intelligent Transportation Systems*, Vol. 20, No. 7, 2019, pp. 2540–2549.
  30. Ghosal, S. S. Travel Time Prediction of Taxis Using Tensor Factorization. *Proc., ACM India Joint International Conference on Data Science and Management of Data, CoDS-COMAD '19*, Kolkata, India, Association for Computing Machinery, New York, 2019.
  31. Gong, S., I. Saadi, J. Teller, and M. Cools. Validation of MCMC-Based Travel Simulation Framework Using Mobile Phone Data. *Frontiers in Future Transportation*, Vol. 2, 2021, p. 10.
  32. Cools, M., E. Moons, and G. Wets. Investigating Effect of Holidays on Daily Traffic Counts: Time Series Approach. *Transportation Research Record: Journal of the Transportation Research Board*, 2007. 2019: 22–31.
  33. Cools, M., E. Moons, and G. Wets. Assessing the Impact of Public Holidays on Travel Time Expenditure: Differentiation by Trip Motive. *Transportation Research Record: Journal of the Transportation Research Board*, 2010. 2157: pp. 29–37.
  34. Kolda, T. G., and B. W. Bader. Tensor Decompositions and Applications. *SIAM Review*, Vol. 51, No. 3, 2009, pp. 455–500.
  35. Kim, Y.-D., and S. Choi. Nonnegative Tucker Decomposition. *Proc., 2007 IEEE Conference on Computer Vision and Pattern Recognition*, IEEE, New York, 2007, pp. 1–8.
  36. Kossaifi, J., Y. Panagakis, A. Anandkumar, and M. Pantic. TensorLy: Tensor Learning in Python. *Journal of Machine Learning Research*, Vol. 20, 2019, pp. 1–6.
  37. Peng, C., X. Jin, K. C. Wong, M. Shi, and P. Liò. Collective Human Mobility Pattern from Taxi Trips in Urban Area. *PLoS One*, Vol. 7, No. 4, 2012, p. 34487.
  38. Christmann, N., M. Mostert, P.-F. Wilmotte, J.-M. Lambotte, and M. Cools. Opportunities for Reinforcing Cross-Border Railway Connections: The Case of the Liège (Belgium)–Maastricht (the Netherlands) Connection. *European Planning Studies*, Vol. 28, No. 1, 2020, pp. 105–124.